

Sticky obstacles to intramolecular energy flow

R. Paškauskas^{1,*}, C. Chandre², and T. Uzer¹

¹ Center for Nonlinear Sciences, School of Physics,

Georgia Institute of Technology, Atlanta, Georgia 30332-0430, U.S.A.

² Centre de Physique Théorique - CNRS, Luminy - Case 907, 13288 Marseille cedex 09, France

(Dated: February 8, 2022)

Vibrational energy flows unevenly in molecules, repeatedly going back and forth between trapping and roaming. We identify bottlenecks between diffusive and chaotic behavior, and describe generic mechanisms of these transitions, taking the carbonyl sulphide molecule OCS as a case study. The bottlenecks are found to be lower-dimensional tori; their bifurcations and unstable manifolds govern the transition mechanisms.

PACS numbers: 34.30.+h, 34.10.+x, 82.20.Db, 82.20.Nk

Chemical reactions usually proceed through a complex choreography of energy flow processes that deliver the needed vibrational energy to the reactive mode. The manner and time in which energy travels determine the outcome of the reaction and the properties of the products. The conventional wisdom concerning this fundamental process is that vibrational energy travels very fast and well before a reaction takes place, distributes itself statistically among the modes of the molecule, assumed to resemble an ensemble of coupled oscillators. Reaction rate theories based on these assumptions - known collectively as statistical theories [1] - have been vindicated in a number of chemical reactions. However, there is increasing evidence that the approach to equilibrium usually proceeds more slowly than predicted by statistical theories [2] - and it is also nonuniform, showing intriguing fits and starts. This anomalous diffusion is caused by variety of phase space structures, such as resonant islands or tori [3] that strongly slow down the trajectories passing nearby [3, 4] and therefore are said to be “sticky” [5]. To date, the theories so successfully applied in pioneering works [6, 7, 8, 9, 10] to lower-dimensional systems have not been extended beyond two degrees of freedom due to severe technical difficulties [11, 12, 13].

The OCS molecule, an important player in greenhouse effect [15], displays the slow and uneven relaxation to statistical equilibrium mentioned above, despite its three strongly coupled degrees of freedom. Models of OCS have served as a testbed for studying intramolecular dynamics in the chaotic regime [16] and these classical findings have been confirmed in parallel quantal wave packet calculations [17]. In this Letter, we investigate vibrational energy flow in the OCS molecule using a Hamiltonian of the form [18]

$$H = T(R_1, R_2, \alpha, P_1, P_2, P_\alpha) + V(R_1, R_2, \alpha), \quad (1)$$

where T is the standard kinetic energy of a rotationless triatomic molecule represented by two interatomic distances R_1 and R_2 , and a bending angle α (with their canonically conjugate momenta P_1 , P_2 and P_α). The

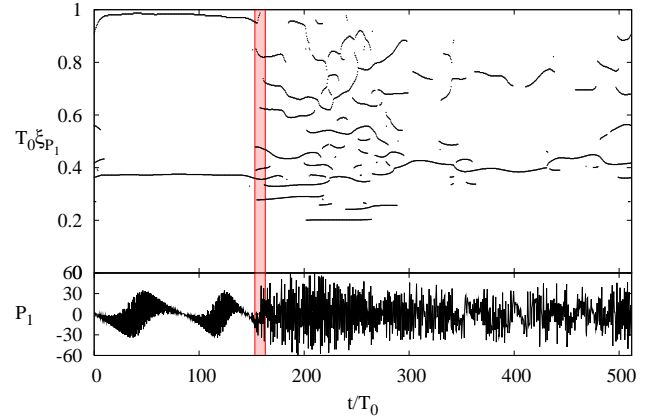


FIG. 1: The generic behavior of chaotic trajectories in Hamiltonian systems involves substantial fraction of intermittent behavior. The time-frequency analysis of a typical OCS trajectory (top panel) allows one to register the transition region (shaded band) and the frequencies ξ of the regular motion, while the time series (lower panel) display the striking features of this abrupt change. t is time (in units of $T_0 = 0.063 \times 10^{-12}$ s) and ξ_{P_1} are the frequency ridges (in units of T_0^{-1}) in the time-frequency decomposition [14] of $P_1(t)$.

potential V is fitted as

$$V(R_1, R_2, \alpha) = \sum_{i=1}^3 V_i(R_i) + V_I(R_1, R_2, R_3), \quad (2)$$

where R_3 is the distance between O and S. The potential consists of Morse potentials V_i for each diatomic pair and an interaction potential V_I of the Sorbie-Murrell form [16]. A rich mixture of chaotic and regular dynamics is observed at energies close to dissociation [19]. The computations below were performed at 90% of the dissociation energy of the weaker bond. Trajectories in the vicinity of a specific periodic orbit with elliptic normal stability are studied, focusing on their escape to the chaotic region, and identifying a generic mechanism of crossover from diffusion [20] to hyperbolicity and chaos.

Figure 1 displays the time series of such a trajectory, initially close to the periodic orbit \mathcal{O}_a with period T_0 (see

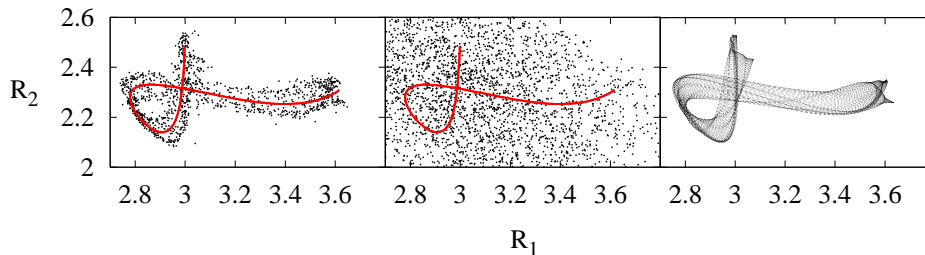


FIG. 2: Projections of the trajectory near a periodic orbit \mathcal{O}_a (with period T_0), analyzed in Fig. 1. The trajectory is represented in (R_1, R_2) plots, broken down into segments, corresponding to the *trapping stage* (left panel) and chaotic stage (center panel). The bottleneck of transition from diffusion to hyperbolicity can be identified as a two-dimensional invariant torus (right panel.) The trajectory is sampled at fixed time intervals $T_0/2$. The orbit \mathcal{O}_a is shown as a solid curve in the center.

Ref. [19]). Figure 2 shows salient features of capture (left panel) followed by an abrupt transition to chaos (center panel). An alternative view of the transition mechanism appears in Fig. 3 in terms of the Poincaré section $\Sigma : P_\alpha = 0, \dot{P}_\alpha > 0, \alpha \leq \pi$. A boundary, marking the crossover from diffusion to hyperbolicity, can be identified in terms of an invariant two-dimensional torus (right panel of Fig. 2). Normal bifurcations of two-dimensional tori turn out to be the key ingredients in the transition mechanism to hyperbolicity, as will be shown below. Generically, there are two stages in the dynamics of the trajectory. During the *trapping stage* (duration t_{trap}), the trajectory is close to (quasi-)periodic, following the unstable manifold of normally hyperbolic tori with very small *positive* Lyapunov exponent (in our case, $\lambda \simeq 10^{-2}$, thus explaining the observed trapping time $t_{\text{trap}} \sim \lambda^{-1}$). During the *escape stage* (duration t_{esc} ; the shaded band in Fig. 1 and “tentacles” in Fig. 3), the trajectory follows the unstable manifolds of the periodic orbit which is in 3:5 resonance with \mathcal{O}_a (thick dots in Fig. 3), with a significantly larger Lyapunov exponent, leading to a fast transition to the chaotic region of phase space (center panel of Fig. 2). These two time scales usually satisfy $t_{\text{trap}} \gg t_{\text{esc}}$. Observations of repeated trapping-escape-chaotic processes in relatively short trajectory segments ($\sim 10^3 T_0$) provide evidence that these effects are prevalent. Dynamical systems theory identifies structures with minimal hyperbolicity as key players in describing long-term features of the chaotic component of an attractor, and integral surfaces with small positive Lyapunov exponent are candidates for the “backbone” of the dynamics. Normally hyperbolic invariant manifolds [21] have recently been implicated in the symbolic dynamics and phase space partition of higher-dimensional chaotic Hamiltonian systems [22, 23], systems with small-dimensional saddles such as the “Crossed Fields” [24] and the Restricted Three Body Problems [25].

Using a combination of trajectory diagnostic tools like Lyapunov maps [19, 26], time-frequency analysis [14], and methods from the theory of dynamical systems like

periodic and quasiperiodic orbit computations [27, 28], we relate the phenomenon of trapping to invariant structures in phase space and to lower-dimensional invariant tori (with a relation to their normal stability properties) in particular. It is commonly assumed that in “typical” Hamiltonian systems with a large number of degrees of freedom N , the relative measure of N -dimensional invariant tori (N local integrals) is either zero or one [29]. The implication is that chaotic systems with large N approach conditions of the stochastic ansatz, and hence, the trapping phenomenon described above is insignificant. On the other hand, it has been established recently that high order resonances form robust islands of secondary structures with positive measure [30].

In order to identify bottlenecks of transition from diffusion to chaos, we monitor the progress of invariant phase space structures along the transition channel using rotation numbers. The results are summarized in Fig. 4, which is central to understanding this transition. In a trapping region around the elliptic periodic orbit \mathcal{O}_a (left panel of Fig. 2), the rotation numbers are obtained from the frequency map analysis [20] on the surface of section. It can be characterized by a single $\omega_{\text{trap}} \approx 0.60556$, implying that a two-dimensional torus is the relevant invariant structure in the trapping process. Having computed a family of two-dimensional tori, parametrized by rotation numbers ω , it is evident that ω_{trap} places the torus on the hyperbolic branch of the bifurcation diagram represented in Fig. 4. This implies that the escape is mediated by manifolds of a torus with hyperbolic normal stability. The duration of the trapping stage is approximately 150 returns on Σ , and is consistent with the maximal Lyapunov exponent $\lambda < 0.05$. Processes associated with the escape from the trapping region can be better understood by analyzing the tangent space of the elliptic periodic orbit \mathcal{O}_a that locally has the structure of a direct product (center + center) $\mathbb{T} \times \mathbb{I}_1 \times \mathbb{T} \times \mathbb{I}_2$, with the periodic orbit at the origin. The elements of the two intervals $\mathbb{I}_i \subset \mathbb{R}$ are rotation numbers ω_i , which are not unique in general: The choice is fixed by requiring

$\lim_{\mu \rightarrow 0} \omega_i = \omega_i^0$, where μ is a measure of the torus and ω_i^0 are stability angles of the elliptic periodic orbit \mathcal{O}_a ($\omega_1^0 = 0.24500633$ and $\omega_2^0 = 0.37046872$). The Poincaré map induces rotations on \mathbb{T} , $r_{\omega_1} \times 1 \times r_{\omega_2} \times 1$, where r_ω is a rotation on \mathbb{T} with the rotation number ω . Partial (or complete) resonances are determined by one (or two) resonance conditions $n\omega_1 + m\omega_2 + k = 0$, where (n, m, k) are integers such that $|n| + |m| + |k| > 0$. The most striking trapping effects are observed for partial resonances of the type $\mathbb{T} \times \mathbb{I}_1 \times \{0\} \times \{0\}$, and $\{0\} \times \{0\} \times \mathbb{T} \times \mathbb{I}_2$. Choosing either of the two situations, a resonance channel has been constructed by finding the two-dimensional invariant tori for $\omega_i \in \mathbb{I}_i$. In order to find these tori we consider the Poincaré map $\mathcal{F}_\Sigma : \Sigma \mapsto \Sigma$. Tori may have hyperbolic normal linear stability, therefore a search for them cannot rely on methods exploiting “stickiness” properties. The sections of two-dimensional invariant tori are one-dimensional closed curves (called hereafter “loops”). We consider loops as discretizations of $\gamma : \mathbb{T} \mapsto \Sigma$ (with periodic boundary condition $\gamma(s) = \gamma(s+1)$) and require that the Poincaré map \mathcal{F}_Σ , restricted to the loop is equivalent to a rigid rotation r_ω . This translates into an invariance condition:

$$\mathcal{F}_\Sigma(\gamma(s)) = \gamma(s + \omega). \quad (3)$$

Equation (3) is solved using damped Newton iterations for the Fourier coefficients of $\gamma(s)$. The linear stability properties of the loop are determined by (Λ, ψ) , solutions of the generalized eigenvalue problem:

$$D\mathcal{F}_\Sigma(s)\psi(s) = \Lambda\psi(s + \omega). \quad (4)$$

Equation (4) has a one-dimensional kernel, which we eliminate using singular value decomposition. The initial data for the Newton iterations $\gamma_0(s)$ and ω were obtained using one of the following two methods: The first method uses the trapping region of the trajectory (see Fig. 1). We estimate ω using Fourier-like methods [20], and truncate the continued fraction expansion of $\omega = [a_1, a_2, \dots]$ before the first large a_i so that $\omega_0 = P/Q$. Then we take sequences of trapping region data every Q iterations and combine them to obtain $\gamma_0(s)$. A refined value of ω can be estimated by minimizing $|\mathcal{F}_\Sigma \circ \gamma_0 - \gamma_0 \circ r_\omega|$. The second method combines continuation in ω with the direct product structure in the neighborhood of the periodic orbit. The surface of section derivative $D\mathcal{F}_\Sigma$ at the periodic orbit has two pairs of complex eigenvalues $\exp[\pm i\omega_i^0]$, $i = 1, 2$. The eigenvectors define mutually skew orthogonal symplectic vector spaces $V_i = \mathbb{R}^2$. It is assumed here that the linear approximation is effective in the neighborhood of the periodic orbit.

The set of two-dimensional tori is found to be discontinuous at the gaps in Fig. 4 due to complete resonances (periodic orbits) and secondary invariant structures. Normal stability is typically elliptic for small $|\omega - \omega_i^0|$. We identify the two-dimensional invariant torus

ω	value	Cont. frac.
ω_A^c	0.240711317575	[4, 6, 2, 11, 5, 5...]
ω_B^c	0.215852976389	[4, 1, 1, 1, 2, 1, 1, 1, 2, 1, 1...]
ω_C^c	0.608654398762	[1, 1, 1, 1, 4, 45, 1, 1, 1, 1...]
ω_D^c	0.605804087926	[1, 1, 1, 1, 6, 3, 2, 2, 1...]

TABLE I: Rotation numbers of the two-dimensional invariant tori at the bifurcation points A, B, C, D shown in Fig. 4.

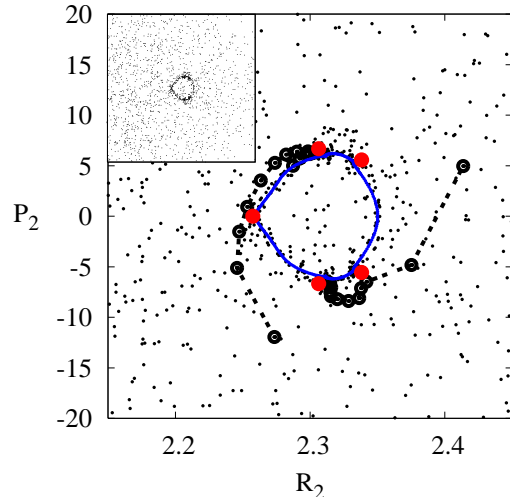


FIG. 3: Poincaré section of the trajectory near a periodic orbit \mathcal{O}_a , analyzed in Figs. 1 and 2. The bottleneck (a two-dimensional torus) is a loop (blue) at the bifurcation point (“D” in Fig. 4). The trajectory is trapped in the vicinity of a loop (which is clearly seen from the inset). The escape stage is shown as two “tentacles,” which extend along the unstable manifolds of a resonant periodic orbit (the five red dots around the center).

at the period doubling bifurcation point as a bottleneck of a given resonance channel. The rationale follows from the theory of dynamical systems: Beyond the bifurcation point at $\omega = \omega^c$, the normal stability changes to hyperbolic. This change affects trajectories passing by its neighborhood. One recurrent observation is that the continued fraction expansion of bifurcation rotation numbers has a tail composed of small integers (see Tab. I). This feature is reminiscent of the observation that the continued fraction expansion of the frequency of the last invariant torus in generic Hamiltonian systems with two degrees of freedom is noble (with a tail of ones) in many situations [6].

The reliability of the numerical solution can be tested by examining its Floquet multipliers, given by Eq. (4). An exact solution consists of a set of complex numbers with up to three different absolute values: 1, Λ , $1/\Lambda$. Significant variation from these values signals an unreliable solution.

In conclusion, our findings indicate that trapping and

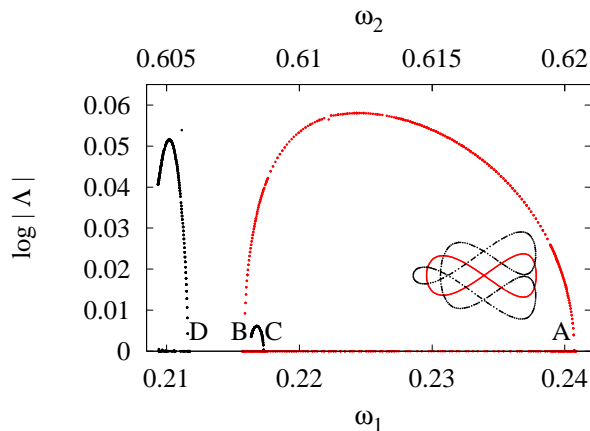


FIG. 4: Fine structure of invariant tori, scanned along the transition channel. The plot shows how Lyapunov exponents depend on the rotation number ω . The points of frequency halving bifurcations (“A”–“D”) can be interpreted as bottlenecks of transition from diffusion to hyperbolicity. Red dots: family of loops arising from the periodic orbit \mathcal{O}_a . Black dots: frequency halved loop, emerging at the bifurcation point “A”. Insets display (R_1, P_1) projections of loops near the bifurcation point “A”. Red: loop with elliptic normal stability and $\omega = \omega_1 \approx 0.24067$. Black: loop with hyperbolic normal stability and $\omega = \omega_2 = (\omega_1 + 1)/2 \approx 0.62033$.

escape are mediated by the same sequence of events, and an approximate boundary, which separates trapped and chaotic behavior, can be found in analogy with the boundaries that separate reactants from products in Transition State Theory [1], where sharply defined phase space structures [24, 31, 32, 33] play this role.

In a broader context, our work forms yet another stimulus to reconsider the relevance of local integrals and partial resonances in realistic, chaotic Hamiltonian systems with many degrees of freedom. Here, we have explained a paradoxical situation, namely that integral surfaces with *positive* Lyapunov exponents (i.e., not “sticky”) can trap chaotic trajectories. Widespread observations of repeated trapping-escape-chaotic processes in short trajectory segments provide evidence that these effects are generic and occurring frequently in many settings ranging from plasmas to celestial mechanics.

This research was partially supported by the US National Science Foundation. C.C. acknowledges support from Euratom-CEA (contract EUR 344-88-1 FUA F).

* Electronic address: rytis@gatech.edu

[1] P. Pechukas, in *Dynamics of Molecular Collisions, Part B*, edited by W. H. Miller (Plenum, N.Y., 1976), chap. 6.

- [2] See, e.g., articles in the Focus Issue *The Fermi-Pasta-Ulam Problem: The First Fifty Years*, *Chaos* **15**(1) (March 2005).
- [3] G. M. Zaslavsky, *Hamiltonian Chaos and Fractional Dynamics* (Oxford University Press, Oxford, 2005).
- [4] A. Semparathi and S. Keshavamurthy, *J. Chem. Phys.* **125**, 141101 (2006).
- [5] A. D. Perry and S. Wiggins, *Physica D* **71**, 102 (1994).
- [6] M. J. Davis, *J. Chem. Phys.* **83**, 1016 (1985).
- [7] M. J. Davis and S. K. Gray, *J. Chem. Phys.* **84**, 5389 (1986).
- [8] S. K. Gray and S. A. Rice, *J. Chem. Phys.* **86**, 2020 (1987).
- [9] C. C. Martens, M. J. Davis, and G. S. Ezra, *Chem. Phys. Lett.* **142**, 519 (1987).
- [10] R. T. Skodje and M. J. Davis, *J. Chem. Phys.* **88**, 2429 (1988).
- [11] R. E. Gillilan, *J. Chem. Phys.* **93**, 5300 (1990).
- [12] R. E. Gillilan and G. S. Ezra, *J. Chem. Phys.* **94**, 2648 (1991).
- [13] M. Toda, *Adv. Chem. Phys.* **130A**, 337 (2005).
- [14] C. Chandre, S. Wiggins, and T. Uzer, *Physica D* **181**, 171 (2003).
- [15] R. P. Turco, R. C. Whitten, O. B. Toon, J. B. Pollack, and P. Hamill, *Nature* **283**, 283 (1980).
- [16] D. Carter and P. Brumer, *J. Chem. Phys.* **77**, 4208 (1982).
- [17] L. L. Gibson, G. C. Schatz, M. A. Ratner, and M. J. Davis, *J. Chem. Phys.* **86**, 3263 (1986).
- [18] A. Foord, J. G. Smith, and D. H. Whiffen, *Mol. Phys.* **29**, 1685 (1975).
- [19] E. Shchekinova, C. Chandre, Y. Lan, and T. Uzer, *J. Chem. Phys.* **121**, 3471 (2004).
- [20] J. Laskar, *Physica D* **67**, 257 (1993).
- [21] M. W. Hirsch, C. C. Pugh, and M. Shub, *Invariant Manifolds* (Springer, N.Y., 1977).
- [22] R. de la Llave, *private communication*.
- [23] R. Paskauskas, *Symbolic dynamics in the Crossed Fields problem*, in preparation.
- [24] T. Uzer, C. Jaffé, J. Palacián, P. Yanguas, and S. Wiggins, *Nonlinearity* **15**, 957 (2002).
- [25] G. Gomez, W. S. Koon, M. W. Lo, J. E. Marsden, J. Mardmont, and S. D. Ross, *Nonlinearity* **17**, 1571 (2004).
- [26] C. Froeschlé, E. Lega, and R. Gonczi, *Celest. Mech. Dyn. Astr.* **67**, 41 (1997).
- [27] C. Simó, in *Modern Methods of Analytical Mechanics and their Applications*, edited by V. V. Rumyantsev and A. V. Karapetyan (Springer, N.Y., 1998), vol. 387 of *CISM Courses and Lectures*.
- [28] À. Jorba, *Nonlinearity* **14**, 943 (2001).
- [29] C. Froeschlé, *Astrophysics and Space Science* **14**, 110 (1971).
- [30] A. Haro and R. de la Llave, *Phys. Rev. Lett.* **85**, 1859 (2000).
- [31] E. Pollak and P. Pechukas, *J. Chem. Phys.* **69**, 1218 (1978).
- [32] R. S. MacKay, *Phys. Lett. A* **145**, 425 (1990).
- [33] R. S. MacKay, *Nonlinearity* **4**, 155 (1991).